Trakya University Journal of Engineering Sciences
http://dergipark.org.tr/tujes
ISSN 2147–0308
Research Article / Araştırma Makalesi
DOI: 10.59314/tujes.1953069

Buckling Analysis of Axially Functionally Graded Tapered Euler-Bernoulli Beams via the Transfer Matrix Method

Vedat TAŞKIN[1]*, Hüseyin Can KILINÇ[1]

[1]*Department of Mechanical Engineering, Trakya University, 22030 Edirne, TÜRKİYE*

Cite this article as: Taşkın, V., Kılınç, H.C. (2026). Buckling Analysis of Axially Functionally Graded Tapered Euler-Bernoulli Beams Via the Transfer Matrix Method. *Trakya University Journal of Engineering Sciences. 27*(1):27-41

Highlights

- Buckling of axially graded tapered beams is solved by the transfer matrix method.
- The fourth-order equation is recast in state-space and integrated by ode45.
- Critical loads are obtained for C-C, C-F, and S-S end conditions.

Article Info

Article History:

Received:
16 May, 2026

Accepted:
9 July, 2026

Keywords:

Transfer matrix method; Axially functionally graded beams; Tapered beams; Buckling analysis; Euler-Bernoulli beam theory.

Abstract

Axially functionally graded (AFG) tapered beams are increasingly used in lightweight structures where stiffness and mass distributions are tailored along the beam axis. The variable-coefficient buckling equation of such beams precludes closed-form solutions and demands numerical treatment. While the finite element method (FEM) is dominant, alternative formulations that bypass element meshing are of interest for benchmarking and parametric studies. In this study, the elastic buckling of double-tapered AFG Euler-Bernoulli beams is solved using the Transfer Matrix Method (TMM). The governing equation is recast in state-space form, and the global transfer matrix is obtained by direct numerical integration. The critical load is the smallest positive root of the boundary-condition-projected characteristic determinant. The formulation is validated against the FEM benchmark for clamped-clamped, clamped-free, and simply-supported boundary conditions, with excellent agreement.

Eksenel Fonksiyonel Derecelendirilmiş Değişken Kesitli Euler-Bernoullı Kirişlerinin Transfer Matrisi Yöntemi ile Burkulma Analizi

Makale Bilgileri

Makale Tarihçesi:

Geliş:
16 Mayıs 2026

Kabul:
9 Temmuz 2026

Anahtar Kelimeler:

Transfer matrisi yöntemi; Eksenel fonksiyonel derecelendirilmiş kirişler; Değişken kesitli kirişler; Burkulma analizi; Euler-Bernoulli kiriş teorisi.

Öz

Eksenel olarak fonksiyonel derecelendirilmiş (AFG) ve iki yönlü değişken kesitli kirişler, rijitlik ile kütlenin eksen boyunca planlı biçimde dağıtıldığı hafif yapısal elemanlarda yaygın olarak kullanılmaktadır. Bu kirişlerin değişken katsayılı burkulma denklemi kapalı-form çözümlere kapalıdır ve sayısal yöntemler gerektirir. Literatürde baskın olan sonlu elemanlar yönteminin yanında, eleman ağı gerektirmeyen alternatif formülasyonlar karşılaştırma kriteri ve parametrik tasarım çalışmaları açısından önemlidir. Bu çalışmada, iki yönlü değişken kesitli AFG Euler-Bernoulli kirişlerinin elastik burkulma problemi Transfer Matrisi Yöntemi (TMM) ile çözülmüştür. Yönetici denklem durum-uzayında yeniden yazılmış; global transfer matrisi doğrudan sayısal entegrasyon ile elde edilmiştir. Kritik yük, sınır koşulu projeksiyonlu karakteristik determinantın en küçük pozitif köküdür. Formülasyon C-C, C-F ve S-S sınır koşulları için FEM çalışması ile karşılaştırılmış ve mükemmel uyum elde edilmiştir.

***Correspondence to:** vedattaskin@trakya.edu.tr

1. Introduction

Functionally graded materials (FGMs) are advanced composites in which the volume fractions of two or more constituents vary continuously over the domain of a body (Birman & Byrd, 2007). The graded microstructure removes the sharp internal interfaces of laminated composites and thereby eliminates the local stress concentrations and delamination paths that limit the load-bearing capacity of conventional layered designs (Koizumi, 1997). Since their introduction, FGMs have been widely adopted in aerospace, automotive, biomedical, and energy applications, motivating an extensive literature on the mechanics of FGM beams, plates and shells (Birman & Byrd, 2007; Sayyad & Ghugal, 2017).

Most early work on FGM beams considered through-thickness variation of the material properties. In a second class of problems, the elastic modulus, the mass density, or both are taken to vary along the beam axis. These axially functionally graded (AFG) beams arise naturally in non-prismatic structural members of aircraft wings, rotor blades, and tapered columns of civil structures, where the axial distribution of stiffness and mass can be tailored to a prescribed loading scenario. The governing equations of AFG beams have variable coefficients, and closed-form solutions exist only for very specific combinations of geometry and material distribution (Elishakoff, 2005; Calió & Elishakoff, 2005; Elishakoff & Endres, 2005).

The semi-inverse approach, advanced by Elishakoff and co-workers, prescribes a polynomial deflection or buckling mode shape and recovers the corresponding distribution of the elastic modulus that satisfies the governing equation and the boundary conditions. The method delivers exact closed-form results for selected mode shapes (Storch & Elishakoff, 2018) but is restrictive: each new combination of boundary conditions or cross-section requires a separate analytical derivation. Singh and Li (2009) and Huang and Li (2010) extended the closed-form analysis to non-uniform AFG columns and beams of varying cross-section, again at the price of problem-specific algebra.

A complementary line of work has focused on numerical methods that accommodate arbitrary distributions of geometry and material. Shahba et al. (2011) proposed a finite element formulation for the free vibration and buckling of AFG tapered Euler-Bernoulli beams, in which the shape functions of homogeneous uniform beam elements are retained and the variable cross-sectional area, moment of inertia, and Young's modulus enter the evaluation of the element stiffness and mass matrices directly. The same group extended the formulation to Timoshenko beams with classical and non-classical end conditions (Shahba et al., 2011b), to tapered beams with axially graded materials (Shahba & Rajasekaran, 2012), and to rotating AFG tapered beams (Zarrinzadeh et al., 2012). Other numerical formulations of the same problem class include the differential transformation element method and the differential quadrature element method (Rajasekaran & Tochaei, 2014), the interpolating matrix method (Liu et al., 2022), hybrid Winkler-Pasternak foundation approaches (Soltani & Asgarian, 2019), the dynamic-stiffness method applied to tapered beams (Banerjee & Ananthapuvirajah, 2018), the asymptotic development method for AFG beams (Cao et al., 2018), and large-deflection analyses of tapered FG beams (Kien & Gan, 2014). All of these methods share the common feature that the beam domain is discretized-into elements, nodes, or interpolation points-before the eigenvalue problem is assembled.

The Transfer Matrix Method (TMM) is a long-established alternative. Originally developed for vibration analysis of multi-bay structures by Pestel and Leckie (1963), TMM recasts a higher-order boundary-value problem as a first-order matrix system on a state vector and propagates the state along the structural axis. The boundary conditions at the two ends of the domain then collapse onto a small characteristic determinant whose roots define the eigenvalues. Because the propagation step is a single initial-value problem on the unit interval, no spatial discretization is required. The method has been applied to the free vibration of variable-cross-section Euler-Bernoulli beams (Boiangiu et al., 2016), to tapered beams (Lee & Lee, 2017), to stepped FGM beams (Liu et al., 2024), and to rotating double-tapered beams (Lee & Lee, 2020).

The buckling problem of axially functionally graded, double-tapered Euler-Bernoulli beams, however, has been addressed predominantly by finite-element and related discretization-based methods. A direct TMM treatment of the same problem-in which the global transfer matrix is obtained by direct numerical integration of the matrix differential equation, without spatial discretization-has received limited attention in the literature, and a side-by-side comparison with the FEM results of Shahba et al. (2011) appears to be unreported.

The objective of the present study is to provide such a TMM formulation and to validate it against the FEM benchmark for all three classical boundary conditions (clamped-clamped, clamped-free, simply supported) over the full range of breadth and height taper ratios considered by Shahba et al. (2011). The remainder of the paper is organized as follows. Section 2 states the problem and the governing equations. Section 3 develops the TMM formulation, including the state-space recast, the global transfer matrix, the boundary-condition projection, the characteristic determinants for the three end conditions, and the numerical algorithm. Section 4 presents the validation results. Section 5 discusses the implications and limitations of the present approach. Section 6 concludes the paper.

Compared with the finite-element benchmark, the present formulation offers three qualitative advantages that are elaborated in Section 5.1. Unlike the finite-element approach, in which the axial variations of the Young's modulus and of the cross-sectional geometry must be represented element by element, the present TMM formulation retains these variations exactly in the system matrix and reduces the buckling eigenvalue problem to the search for a single sign change of a 2×2 characteristic determinant. No mesh-refinement study is required, since convergence is controlled adaptively by the error tolerances of the underlying ODE solver rather than by a user-supplied spatial discretization parameter.

2. Problem Definition

Consider a straight, double-tapered, axially functionally graded (AFG) beam of length L under the action of an axial compressive end load P, as illustrated in Fig. 1. Let X denote the coordinate along the beam axis with the origin placed at the left end (X = 0) and the right end at X = L. Following Shahba et al. (2011), the breadth and the height of the rectangular cross-section vary linearly along the beam axis as

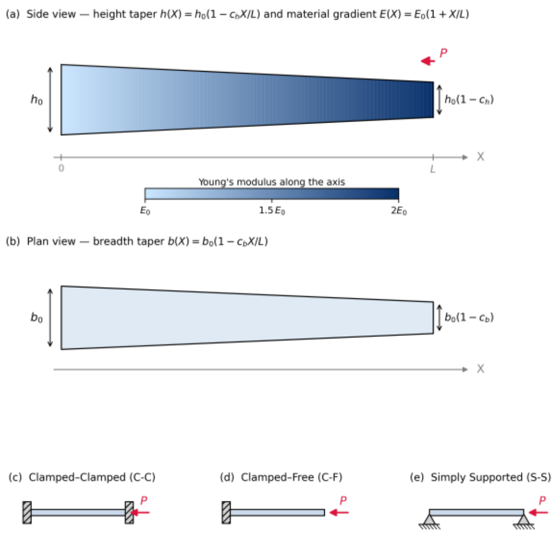

Figure 1. Geometry and boundary conditions of the AFG double-tapered Euler-Bernoulli beam: (a) side view; (b) plan view; (c)–(e) schematics of the three classical boundary-condition cases CC, CF, and SS

$$b(X) = b_0\left(1 - c_b\frac{X}{L}\right), h(X) = h_0\left(1 - c_h\frac{X}{L}\right) \quad (1)$$

where b_0 and h_0 are the breadth and the height at X = 0, and cb ∈ [0, 1] and ch ∈ [0, 1] are the breadth and the height taper ratios, respectively. The cross-sectional area and the second moment of area then take the form

$$A(X) = A_0\left(1 - c_b\frac{X}{L}\right)\left(1 - c_h\frac{X}{L}\right),$$
$$I(X) = I_0\left(1 - c_b\frac{X}{L}\right)\left(1 - c_h\frac{X}{L}\right)^3 \quad (2)$$

with $A_0 = b_0 h_0$ and $I_0 = b_0 h_0^3 / 12$ being the cross-sectional area and the second moment of area at X=0. Setting cb=ch=0 reduces Eq. (2) to a prismatic beam, while cb=ch=1 describes the theoretical limit of a beam tapering to a point at X=L.

The axial functional grading is introduced through a linear distribution of Young's modulus along the beam axis,

$$E(X) = E_0\left(1 + \frac{X}{L}\right) \quad (3)$$

where E_0 is the value at X = 0. The Poisson ratio is taken to be constant and is not required for the buckling analysis considered in the present study. The mass density distribution does not enter the buckling problem and is therefore not specified here.

Under the assumptions of the classical Euler-Bernoulli beam theory (planar deformation, plane sections remain plane and normal to the deformed axis, small deflections, linear elastic behavior), the equilibrium of the laterally deflected beam under the constant axial compressive load P is governed by

$$\frac{d^2}{dX^2}\left[E(X)I(X)\frac{d^2w}{dX^2}\right] + P\frac{d^2w}{dX^2} = 0, 0 \le X \le L \quad (4)$$

where w(X) is the lateral (transverse) deflection.

The three sets of classical boundary conditions used in the present study are:

- Clamped-Clamped (C-C): w(0) = w′(0) = w(L) = w′(L) = 0
- Clamped-Free (C-F): w(0) = w′(0) = 0 and M(L) = V(L) = 0
- Simply Supported (S-S): w(0) = M(0) = w(L) = M(L) = 0

where the prime denotes differentiation with respect to X, M(X) = E(X) I(X) w″(X) is the bending moment, and V(X) = dM/dX − P w′(X) is the transverse shear force consistent with the equilibrium of a deflected column under axial compression (Reddy, 2017).

The objective of the analysis is to determine the smallest value of P -termed the critical buckling load P_{cr} -for which Eq. (4) admits a non-trivial solution w(X) satisfying the prescribed boundary conditions. To facilitate the comparison of results across different geometries and material distributions, the critical load is reported in the non-dimensional form

$$\lambda = \frac{P_{cr}L^2}{E_0 I_0} \quad (5)$$

which is the convention adopted by Shahba et al. (2011) and is followed here.

For the subsequent treatment, it is convenient to introduce the non-dimensional axial coordinate

$$\xi = \frac{X}{L}, \xi \in [0,1] \quad (6)$$

so that the geometric and material distributions of Eqs. (2)–(3) become

$$\begin{aligned} g_b(\xi) &= 1 - c_b\xi, \\ g_h(\xi) &= 1 - c_h\xi, \\ g_A(\xi) &= g_b(\xi)g_h(\xi), \\ g_I(\xi) &= g_b(\xi)g_h(\xi)^3, \\ g_E(\xi) &= 1 + \xi \end{aligned} \quad (7)$$

In terms of these dimensionless distribution functions, the cross-sectional rigidity is

$$E(X)I(X) = E_0 I_0 g_E(\xi) g_I(\xi) \quad (8)$$

and Eq. (4) takes the dimensionless form

$$\frac{d^2}{d\xi^2}\left[g_E(\xi)g_I(\xi)\frac{d^2w}{d\xi^2}\right] + \lambda\frac{d^2w}{d\xi^2} = 0, \xi \in [0,1] \quad (9)$$

where λ is the non-dimensional axial load defined by Eq. (5). Equation (9) is the variable-coefficient ordinary differential equation whose lowest eigenvalue λ_{cr} corresponds to the critical buckling state of the beam and is sought in the present study.

3. Transfer Matrix Method (TMM) Formulation

The Transfer Matrix Method recasts an n-th order ordinary differential equation as a system of n first-order equations on a state vector. The transfer matrix maps the state at one end of the beam onto the state at the other end. Once the global transfer matrix is known, the boundary conditions yield a characteristic determinant whose smallest positive root defines λ_{cr}.

3.1. State-Space Representation

The bending moment and the effective shear force in the deflected column are

$$\begin{aligned} M(X) &= E(X)I(X)w''(X), \\ V(X) &= M'(X) - Pw'(X) \end{aligned} \tag{10}$$

The second term in V(X) accounts for the contribution of the axial load P to the transverse equilibrium. Combining Eq. (10) with the governing Eq. (4) gives

$$V'(X) = 0, M'(X) = V(X) + Pw'(X) \tag{11}$$

and the moment definition itself supplies

$$w''(X) = \frac{M(X)}{E(X)I(X)} \tag{12}$$

Equations (11)–(12), together with w′=w′, are four first-order equations on the state variables w, w′, M, V. With the dimensionless coordinate ξ= X/L, the dimensionless state vector

$$Z(\xi) = [w(\xi), w'(\xi), M^*(\xi), V^*(\xi)]^T \tag{13}$$

and the dimensionless moment and shear

$$M^* = \frac{ML}{E_0 I_0}, V^* = \frac{VL^2}{E_0 I_0} \tag{14}$$

the system takes the compact form

$$\frac{dZ}{d\xi} = A(\xi;\lambda)Z(\xi), \xi \in [0,1] \tag{15}$$

with the system matrix

$$A(\xi;\lambda) = \begin{pmatrix} 0 & 1 & 0 & 0 \\ 0 & 0 & -\frac{1}{g_E(\xi)g_I(\xi)} & 0 \\ 0 & \lambda & 0 & 1 \\ 0 & 0 & 0 & 0 \end{pmatrix} \tag{16}$$

The dimensionless rigidity $g_E(\xi)$ $g_I(\xi)$ is given by Eqs. (7)–(8). The last row of A vanishes because the dimensionless shear is constant in the absence of distributed transverse loads (Eq. 11, first relation).

3.2. Definition of the Transfer Matrix

The transfer matrix T(ξ) is the fundamental matrix solution of Eq. (15) satisfying T(0) = I. It obeys

$$\frac{dT(\xi)}{d\xi} = A(\xi;\lambda)T(\xi), T(0) = I \tag{17}$$

and propagates the state from the left end to any section ξ:

$$Z(\xi) = T(\xi)Z(0) \tag{18}$$

At ξ=1 we obtain the global transfer matrix T_L = T(1):

$$Z(1) = T_L Z(0) \tag{19}$$

For a prismatic, homogeneous beam (cb = ch = 0, $g_E \equiv 1$), A is constant and T_L admits a closed-form matrix exponential. For the general AFG tapered case, the coefficients are variable and T_L must be evaluated numerically. The numerical procedure is described in Section 3.5.

3.3. Boundary-Condition Projection and Characteristic Equation

At ξ = 0 and ξ = 1, each of the three classical boundary conditions (C-C, C-F, S-S) prescribes two components of the state vector Z and leaves the other two unknown. Inserting these constraints into Eq. (19) yields a homogeneous 2×2 linear system on the two unknown components of Z(0). A non-trivial solution exists only when the determinant of this 2×2 system vanishes, which gives the characteristic equation for λ.

Let Z = [w, w′, M*, V*]^T as in Eq. (13), and let the global transfer matrix be written component-wise as T_L = [T_{ij}], i, j = 1…4. For each boundary-condition case the columns of T_L are selected according to the unknown components of Z(0), while the rows are selected according to the zero-target components of Z(1).

Clamped-Clamped (C-C). Writing the first two rows of Eq. (19) and using $Z_1(0) = Z_2(0) = 0$,

$$\begin{pmatrix} w(1) \\ w'(1) \end{pmatrix} = \begin{pmatrix} T_{13} & T_{14} \\ T_{23} & T_{24} \end{pmatrix} \begin{pmatrix} M^*(0) \\ V^*(0) \end{pmatrix} = \begin{pmatrix} 0 \\ 0 \end{pmatrix} \quad (20)$$

so the characteristic determinant is

$$D_{CC}(\lambda) = T_{13}T_{24} - T_{14}T_{23} \quad (21)$$

Clamped-Free (C-F). Using the third and the fourth rows of Eq. (19),

$$\begin{pmatrix} M^*(1) \\ V^*(1) \end{pmatrix} = \begin{pmatrix} T_{33} & T_{34} \\ T_{43} & T_{44} \end{pmatrix} \begin{pmatrix} M^*(0) \\ V^*(0) \end{pmatrix} = \begin{pmatrix} 0 \\ 0 \end{pmatrix} \quad (22)$$

giving

$$D_{CF}(\lambda) = T_{33}T_{44} - T_{34}T_{43} \quad (23)$$

Simply Supported (S-S). Using the first and the third rows of Eq. (19),

$$\begin{pmatrix} w(1) \\ M^*(1) \end{pmatrix} = \begin{pmatrix} T_{12} & T_{14} \\ T_{32} & T_{34} \end{pmatrix} \begin{pmatrix} w'(0) \\ V^*(0) \end{pmatrix} = \begin{pmatrix} 0 \\ 0 \end{pmatrix} \quad (24)$$

so

$$D_{SS}(\lambda) = T_{12}T_{34} - T_{14}T_{32} \quad (25)$$

3.4. Critical Load as the Lowest Eigenvalue

For each boundary-condition case, the buckling problem reduces to an eigenvalue problem for λ defined by the characteristic equation

$$D_{BC}(\lambda) = 0, BC \in \{C\text{-}C, C\text{-}F, S\text{-}S\} \quad (26)$$

The critical (dimensionless) buckling load is the lowest eigenvalue of this problem:

$$\lambda_{cr} = \min\{\lambda > 0: D_{BC}(\lambda) = 0\} \quad (27)$$

Higher eigenvalues of Eq. (26) correspond to higher buckling modes. The dimensional critical load follows from Eq. (5):

$$P_{cr} = \frac{\lambda_{cr} E_0 I_0}{L^2} \quad (28)$$

3.5. Numerical Evaluation of the Global Transfer Matrix

Equation (17) is a 4×4 matrix-valued initial-value problem on $\xi \in [0, 1]$. The matrix $T(\xi)$ is unfolded column-by-column into a vector of length 16, so that the matrix equation is integrated as a system of sixteen scalar first-order ordinary differential equations with the initial condition $T(0) = I$. At each step, the product $A(\xi; \lambda) \cdot T(\xi)$ is formed directly and reshaped into the derivative vector.

The scalar system is integrated from $\xi = 0$ to $\xi = 1$ using the MATLAB function ode45, a variable-step Runge-Kutta solver of order (4,5) (Shampine & Reichelt, 1997). The relative and absolute error tolerances are set to RelTol=10^{-9} and AbsTol=10^{-10}, respectively. The solution at $\xi = 1$ is reshaped back into the 4×4 global transfer matrix T_L. The cost of one such integration is independent of any spatial discretization, which is one of the main practical advantages of the TMM over mesh-based methods.

3.6. Determination of λ_{cr}

For a fixed boundary-condition case and a fixed pair of taper ratios (cb, ch), the characteristic determinant $D_{BC}(\lambda)$ defined by Eqs. (21), (23) or (25) is a real-analytic function of λ whose zeros correspond to the buckling eigenvalues of the column. The lowest such eigenvalue, λ_{cr}, is determined in two steps.

Step 1 — Coarse scan. The interval $\lambda \in [\lambda_{min}, \lambda_{max}]$ is discretized into N uniformly spaced sample points, and $D_{BC}(\lambda)$ is evaluated at each point by integrating Eq. (17) and assembling the corresponding 2×2 sub-matrix. The first sign change of $D_{BC}(\lambda)$ brackets the lowest positive root. The scan range is chosen separately for each boundary-condition case to enclose the expected first eigenvalue with margin: $\lambda \in [0.05, 30]$ for C-F, $\lambda \in [0.5, 60]$ for S-S, and $\lambda \in [0.5, 200]$ for C-C, with N = 1200 to 1600 sample points.

Step 2 — Refinement. Once a sign-change bracket $[\lambda_k, \lambda_{\{k+1\}}]$ containing λ_{cr} is identified, the MATLAB function fzero, a hybrid root-finder, is invoked on the same characteristic determinant. The convergence tolerance is set to $\mathrm{TolX} = 10^{-9}$.

The two-step strategy decouples root isolation from root refinement: the coarse scan reliably brackets the lowest root even when the characteristic determinant is steep or oscillatory, while fzero delivers high accuracy at minimal additional cost.

3.7. Algorithmic Summary

The complete procedure for computing the dimensionless critical buckling load λ_{cr} for a prescribed boundary condition BC and taper-ratio pair (cb, ch) is summarized in Algorithm 1.

Algorithm 1—TMM solution of the AFG tapered Euler-Bernoulli buckling problem

Input: cb, ch, BC, λ scan range $[\lambda_{min}, \lambda_{max}]$, N
Output: λ_{cr}
1. define $A(\xi;\lambda)$ by Eq.(16), with $g_E(\xi)$, $g_I(\xi)$ from Eq.(7)
2. define function $D_{BC}(\lambda)$:
integrate $dT/d\xi = A(\xi;\lambda)\ T$ over $[0,1]$ with $T(0)=I$
extract the 2×2 sub-matrix $R(\lambda)$ according to BC (Eqs.20-25) return $\det R(\lambda)$
3. generate λ-scan vector $\lambda_k = \lambda_{min} + (k-1)(\lambda_{max} - \lambda_{min})/(N-1)$, k = 1…N
4. evaluate $d_k = D_{BC}(\lambda_k)$ for k = 1…N
5. locate smallest k* such that $\mathrm{sign}(d_{\{k^*\}}) \neq \mathrm{sign}(d_{\{k^*+1\}})$
6. $\lambda_{cr} \leftarrow \mathrm{fzero}(D_{BC}, [\lambda_{\{k^*\}}, \lambda_{\{k^*+1\}}])$
7. return λ_{cr}

The inner ODE integration invoked at Steps 4 and 6 is the dominant computational cost of the algorithm. The total cost is linear in N (one integration per scan point) plus the cost of a small number of additional integrations during the fzero refinement. The procedure requires no spatial mesh and no assembly of stiffness or geometric-stiffness matrices. A flowchart corresponding to Algorithm 1 is given in Fig. 2.

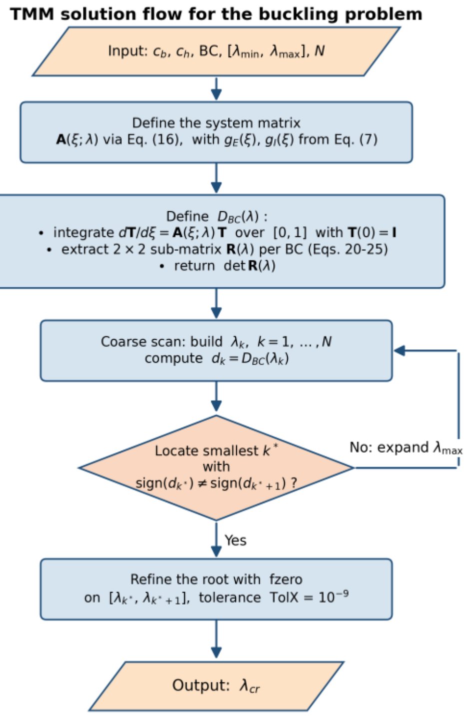

Figure 2. Flowchart of the TMM algorithm (Algorithm 1) for the AFG tapered Euler-Bernoulli buckling problem.

4. Numerical Validation and Results

The TMM formulation developed in Section 3 is implemented in MATLAB R2025a, and all computations reported in this section are performed with this implementation. The formulation is validated against the finite-element benchmark of Shahba et al. (2011), in which the same beam problem is discretized into 20 equal-length elements and the resulting eigenvalue problem is solved by standard linear algebra. The benchmark covers double-tapered, axially functionally graded Euler-Bernoulli beams with the geometry of Eq. (2), the linear Young's modulus distribution of Eq. (3), and three classical boundary conditions: clamped-clamped (C-C), clamped-free (C-F), and simply supported (S-S). The breadth and the height taper ratios are each varied over the set cb, ch ∈ {0.0, 0.2, 0.4, 0.6, 0.8}, yielding twenty-five geometric configurations per boundary-condition case.

For every configuration, the dimensionless critical buckling load λ_{cr} is computed by the procedure of

Algorithm 1. Tables 1–3 report the present TMM results alongside the corresponding FEM values of Shahba et al. (2011) for the C-C, C-F, and S-S cases, respectively.

4.1. Clamped-Clamped Beams

For the C-C case, the critical load λ_{cr} is largest for the uniform beam (cb = ch = 0) and decreases as either taper ratio is increased. The dependence on the height taper ratio ch is markedly stronger than that on the breadth taper ratio cb, because ch enters the moment of inertia in Eq. (2) cubically while cb enters linearly. At the extreme of cb = ch = 0.8 the critical load drops to about 4.5 % of its value at the uniform configuration. The present TMM and the reference FEM values agree across the entire (cb, ch) grid, as shown in Table 1.

Table 1: Non-dimensional critical buckling load λ_{cr} for C-C AFG tapered beams.

	ch = 0.0		**ch = 0.2**		**ch = 0.4**		**ch = 0.6**		**ch = 0.8**	
cb	**Present**	***FEM***	**Present**	***FEM***	**Present**	***FEM***	**Present**	***FEM***	**Present**	***FEM***
0.0	57.3945	57.3948	41.9171	41.9174	28.1795	28.1798	16.3413	16.3416	6.6809	6.6812
0.2	51.7860	51.7863	37.6025	37.6028	25.0891	25.0894	14.3960	14.3963	5.7843	5.7847
0.4	45.7359	45.7362	32.9640	32.9643	21.7814	21.7817	12.3268	12.3271	4.8407	4.8410
0.6	38.9917	38.9921	27.8172	27.8175	18.1333	18.1336	10.0642	10.0645	3.8237	3.8240
0.8	30.8922	30.8925	21.6803	21.6806	13.8243	13.8247	7.4279	7.4282	2.6662	2.6665

4.2. Clamped-Free Beams

The C-F case has the lowest absolute critical loads among the three end conditions, in agreement with the classical Euler hierarchy of column stability (Timoshenko & Gere, 1961). The qualitative trends with respect to cb and ch are the same as in the C-C case: λ_{cr} decreases monotonically with either taper ratio, with a steeper sensitivity to ch. The agreement between the present TMM results and the FEM benchmark is excellent throughout the (cb, ch) grid, as displayed in Table 2.

Table 2: Non-dimensional critical buckling load λ_{cr} for C-F AFG tapered beams.

	ch = 0.0		**ch = 0.2**		**ch = 0.4**		**ch = 0.6**		**ch = 0.8**	
cb	**Present**	***FEM***	**Present**	***FEM***	**Present**	***FEM***	**Present**	***FEM***	**Present**	***FEM***
0.0	3.1173	3.1177	2.6222	2.6225	2.1051	2.1054	1.549	1.5522	0.9242	0.9245
0.2	2.9493	2.9497	2.4635	2.4638	1.9582	1.9585	1.414	1.4217	0.8214	0.8217
0.4	2.7674	2.7676	2.2912	2.2915	1.7985	1.7988	1.2795	1.2798	0.7106	0.7109
0.6	2.5649	2.5652	2.0989	2.0992	1.6197	1.6200	1.1205	1.1208	0.5880	0.5883
0.8	2.3282	2.3285	1.8722	1.8725	1.4071	1.4074	0.9306	0.9309	0.4438	0.4441

4.3. Simply Supported Beams

For the S-S case the critical loads fall between the C-F and C-C extremes, again consistent with the classical hierarchy. The cb/ch trends mirror the previous two cases. The TMM results reproduce the FEM benchmark over the full grid, as shown in Table 3.

Table 3: Non-dimensional critical buckling load λ_{cr} for S-S AFG tapered beams.

	ch = 0.0		ch = 0.2		ch = 0.4		ch = 0.6		ch = 0.8	
cb	**Present**	***FEM***	**Present**	***FEM***	**Present**	***FEM***	**Present**	***FEM***	**Present**	***FEM***
0.0	14.5110	14.5113	10.6857	10.6860	7.2828	7.2831	4.3284	4.3287	1.8556	1.8559
0.2	13.1395	13.1398	9.5968	9.5971	6.4712	6.4715	3.7889	3.7892	1.5949	1.5952
0.4	11.6966	11.6969	8.4540	8.4543	5.6225	5.6228	3.2281	3.2284	1.3156	1.3159
0.6	10.1448	10.1451	7.2285	7.2288	4.7161	4.7164	2.6335	2.6338	1.0239	1.0242
0.8	8.3954	8.3957	5.8496	5.8499	3.7016	3.7019	1.9746	1.9749	0.7076	0.7078

4.4. Overall Observations

Across all three boundary-condition cases and twenty-five geometric configurations per case, the present TMM formulation reproduces the FEM benchmark of Shahba et al. (2011) to excellent accuracy. The agreement is uniform: it does not deteriorate at the extreme corners of the taper-ratio grid where the cross-section approaches a near-point limit, nor does it depend on the boundary-condition case. This uniformity is a direct consequence of the mesh-free character of the TMM: the same ode45 integration is used for every (cb, ch, BC) combination, with no element-discretization choice intervening between the geometry and the eigenvalue.

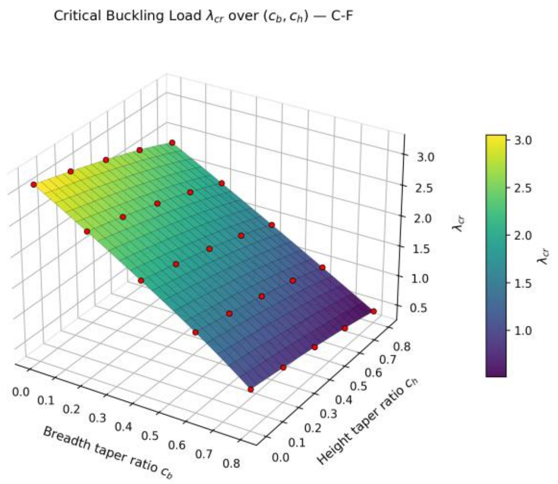

Figure 4. λ_{cr} surface over the (cb, ch) plane for the CF case.

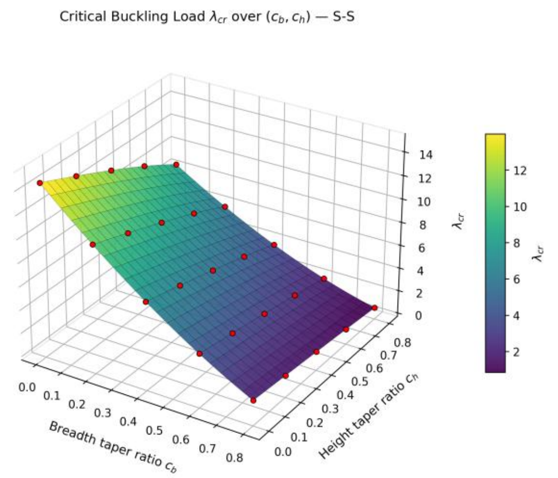

Figure 5. λ_{cr} surface over the (cb,ch) plane for the SS case.

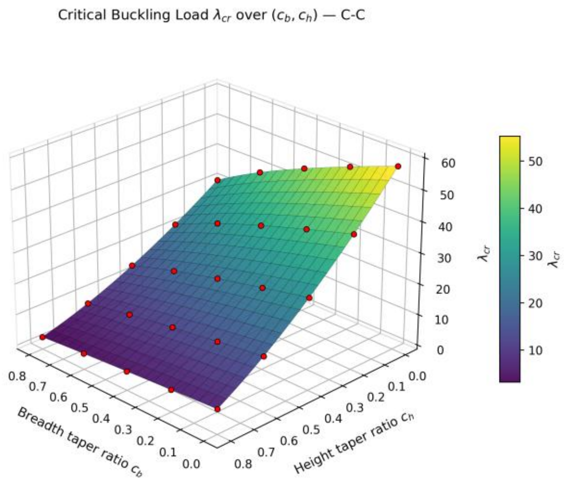

Figure 3. λ_{cr} surface over the (cb, ch) plane for the CC case.

In addition to the tabulated results, Figs. 3–5 display the surface of λ_{cr} over the (cb, ch) plane for the C-C, C-F, and S-S cases, respectively. The surfaces are monotone-decreasing in both cb and ch, with the height-taper sensitivity clearly dominating, and exhibit no spurious oscillations or local artefacts.

4.5. Buckling Mode Shapes

The buckling mode shapes corresponding to the first three eigenvalues of the characteristic equation are obtained as follows. For each (cb, ch, BC) configuration and each eigenvalue λ_k, the boundary-condition-projected 2 × 2 matrix $R(\lambda_k)$ defined in Section 3.3 is singular. The right null-vector of $R(\lambda_k)$ supplies the unknown components of the initial state $Z(0)$; the remaining components are zero by the prescribed kinematic constraints. Forward integration of Eq. (15) from $\xi = 0$ to $\xi = 1$ with this assembled initial state yields the deflection $w(\xi)$ along the beam, which is then peak-normalized for plotting.

Figs. 6–8 display the first three buckling mode shapes for the C-C, C-F, and S-S boundary conditions, respectively, for two configurations per figure: the uniform reference case (cb = ch = 0.0) and a severely tapered case (cb = ch = 0.8). The corresponding dimensionless critical loads λ_k are reported in the legends.

For the C-C case (Fig. 6), the mode shapes preserve the classical clamped-clamped symmetry pattern ($n - 1$ internal nodes for the n-th mode), although the AFG stiffening of the material along the axis shifts the antinodes slightly toward the stiffer end. For the C-F case (Fig. 7), the cantilever mode shapes follow the canonical pattern, with the deflection growing from the clamped root toward the free tip. For the S-S case (Fig. 8), the mode shapes are reminiscent of the classical sinusoidal modes of a uniform pinned-pinned column, again with mild asymmetry induced by the axial gradient. In all three boundary-condition cases, the severely tapered configuration produces qualitatively similar mode shapes but at substantially lower critical loads, in agreement with the trends of Tables 1–3.

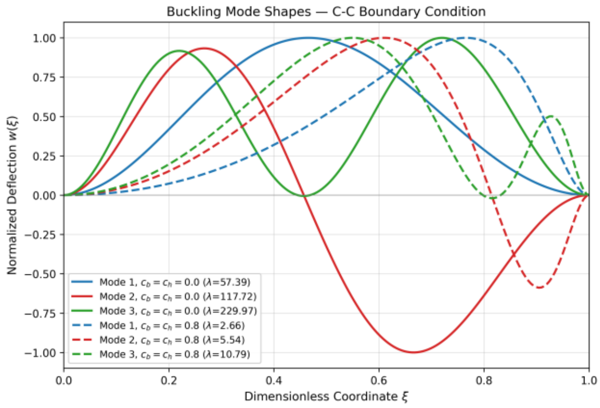

Figure 6. First three buckling mode shapes for the C-C case: uniform (cb=ch=0.0) and severely tapered (cb=ch=0.8) configurations.

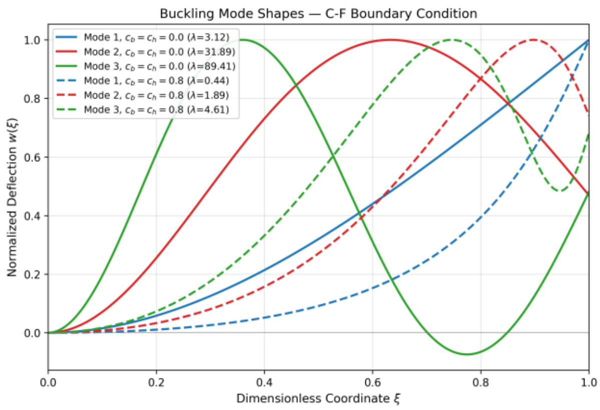

Figure 7. First three buckling mode shapes for the CF case: uniform (cb=ch=0.0) and severely tapered (cb=ch=0.8) configurations.

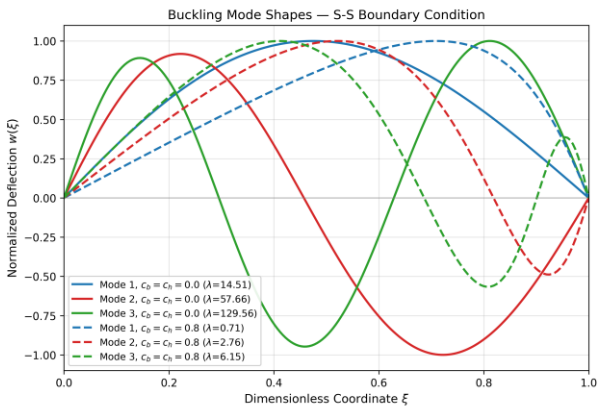

Figure 8. First three buckling mode shapes for the S-S case: uniform (cb=ch=0.0) and severely tapered (cb=ch=0.8) configurations.

5. Discussion

5.1. Comparison with the Finite Element Formulation

The TMM formulation developed in the present study differs from the finite-element formulation of Shahba et al. (2011) in three closely related respects, each of which offers a specific practical advantage for the axially functionally graded (AFG) double-tapered buckling problem: the absence of any spatial discretization parameter, the reduced algebraic size of the resulting eigenvalue problem, and the direct treatment of the axial variations of the material and geometric properties.

First, the present formulation is mesh-free. In the FEM benchmark of Shahba et al. (2011), the beam is discretized into twenty equal-length Hermite-cubic elements, and the choice of this element count is a modelling decision left to the practitioner; changing it modifies the computed critical load and, in principle, requires a separate convergence study. In the present formulation there is no analogue of an element count. The state vector $Z(\xi)$ is propagated over the unit interval by a single ODE integration whose accuracy is controlled by the relative and absolute tolerances of ode45 (10^{-9} and 10^{-10}, respectively). Adaptive step selection concentrates integration points automatically in regions where the state variables vary most rapidly, so that convergence is achieved without any user-supplied spatial discretization parameter. This property is particularly valuable at large taper ratios, where the cross-section tends to vanish toward the tapered end and where a uniform FEM mesh would call for local refinement to resolve the associated stiffness gradient.

Second, the algebraic size of the buckling eigenvalue problem is considerably smaller in the TMM formulation. A twenty-element Hermite-cubic FEM discretization of the AFG tapered beam yields a generalized eigenvalue problem of the form $(K - \lambda K_G) \varphi = 0$, whose stiffness and geometric-stiffness matrices are of order approximately forty after imposition of the boundary conditions. In the present TMM formulation, each evaluation of the characteristic determinant requires the integration of only sixteen scalar first-order ordinary differential equations, and the buckling condition itself reduces to the vanishing of the determinant of a single 2×2 sub-matrix of the global transfer matrix, as expressed in Eqs. (21), (23) and (25). The eigenvalue problem is therefore recast as a scalar root-finding problem rather than as an algebraic generalized eigenvalue problem, which also simplifies the numerical extraction of the higher buckling modes reported in Section 4.5.

Third, and most importantly for the AFG tapered class of problems considered here, the axial distributions of the Young's modulus $E(\xi)$ and of the cross-sectional dimensions $b(\xi)$ and $h(\xi)$ enter the system matrix $A(\xi;\lambda)$ directly, without any intra-element approximation. In an element-based formulation these distributions are necessarily represented within each element either as element-averaged constants or by low-order polynomials, so that a residual modelling error is introduced independently of the mesh density. In the present formulation the analytical distribution functions given by Eqs. (7) are sampled directly by the ODE solver at the integration points selected by its own error estimator, and the only source of approximation is that of the ODE integrator itself. This observation explains, in retrospect, why the TMM results reported in Section 4 reproduce the FEM benchmark uniformly to four decimal places over the entire (cb, ch) grid: the two formulations agree not because the FEM discretization is exact, but because at twenty elements the residual modelling error of the FEM approximation is already smaller than the reporting precision. For AFG members with more strongly varying material or geometric distributions the same FEM discretization would require additional refinement to preserve this level of agreement, whereas the TMM formulation would require no modification.

5.2. Effect of Geometric Tapering

The numerical results of Section 4 confirm two qualitative trends that follow from the underlying Eqs. (2) and (4). First, the height taper ratio ch has a markedly stronger effect on the critical load than the breadth taper ratio cb, because ch enters the moment of inertia cubically while cb enters linearly. Second, the relative ordering of the three boundary-condition cases - C-F < S-S < C-C - is preserved across the entire (cb, ch) grid, consistent with the classical Euler hierarchy for prismatic columns. The mode-shape plots of Figs. 6–8 further show that, for each boundary-condition case, severe tapering reduces the critical load by more than an order of magnitude while leaving the qualitative shape of the deflection profile essentially unchanged.

This behaviour has a straightforward mechanical origin. The second moment of area of a rectangular cross-section depends linearly on the breadth $b(\xi)$ but cubically on the height $h(\xi)$, so that an incremental reduction of h at any axial station produces three times the relative reduction of the local moment of inertia caused by the same relative reduction of b. Since buckling is governed by the axial distribution of the bending rigidity $E(\xi)I(\xi)$, and since the sections of lowest local rigidity dominate the eigenvalue problem, the cumulative stiffness deficit introduced by tapering the height is much larger than that introduced by tapering the breadth. This is the reason for the pronounced asymmetry between the c_h - and c_b sensitivities of λ_{cr} observed in Tables 1–3 and Figs. 3–5.

The axial grading of the Young's modulus prescribed by Eq. (3) acts in the direction opposite to the geometric tapering, since the stiffer material is placed precisely where the cross-section is smaller. The product $E(\xi)I(\xi)$ that enters the governing equation therefore reflects two competing axial effects — geometric stiffness loss and material stiffness gain — and this partial compensation is what keeps λ_{cr} finite and non-zero even at severe taper ratios such as $c_h = 0.8$. Since the present problem is that of static elastic buckling, the mass density does not appear in Eq. (4) and the mass distribution of the AFG beam does not influence the results reported here; the discussion above therefore concerns the effect of the cross-sectional variation on the rigidity distribution only.

5.3. Limitations and Scope

The present formulation rests on three classical assumptions: (i) the Euler-Bernoulli kinematics (plane sections remain plane and normal to the deformed axis), which neglects transverse shear deformation and rotary inertia; (ii) linear elastic material behavior; and (iii) small deflections of the beam axis. Extensions to Timoshenko kinematics, to higher-order shear deformation theories, or to geometric nonlinearity would change the order of the governing equation and the dimension of the state vector but would leave the overall TMM workflow-state-space recast, transfer matrix by ode integration, boundary-condition projection, characteristic determinant-unchanged. These extensions are outside the scope of the present study.

6. Conclusions

The Transfer Matrix Method has been applied to the elastic buckling problem of double-tapered, axially functionally graded Euler-Bernoulli beams. The fourth-order governing equation with variable coefficients was recast in state-space form on the four state components w, w', M^*, V^*; the global transfer matrix was obtained by direct numerical integration of the matrix differential equation; and the critical buckling load was identified as the lowest eigenvalue of the boundary-condition-projected characteristic determinant. The formulation accommodates clamped-clamped, clamped-free, and simply supported end conditions through different 2×2 projections of the same global transfer matrix, with no change in the inner integration procedure.

The TMM results were validated against the finite element benchmark of Shahba et al. (2011) over the full grid of breadth and height taper ratios for all three boundary-condition cases. The agreement is uniform and excellent across the entire grid, including the severely tapered corners. The accompanying mode-shape plots reveal that the first three buckling modes preserve their canonical structure even under severe geometric tapering, while the corresponding eigenvalues are reduced by more than an order of magnitude.

The principal practical advantages of the TMM formulation in this problem class are threefold. First, the algorithm is mesh-free: a single ODE integration over the unit interval, adaptively controlled by the tolerances of ode45, suffices to propagate the state vector, and no user-supplied spatial discretization parameter is required. Second, the buckling condition reduces to the search for the lowest root of a single scalar characteristic equation involving the determinant of a 2×2 sub-matrix of the global transfer matrix, in contrast to the approximately forty-DoF generalized eigenvalue problem that arises from a comparable twenty-element finite-element discretization. Third, and most importantly, the axial variations of the Young's modulus and of the cross-sectional dimensions enter the system matrix directly, so that no intra-element polynomial approximation of these distributions is introduced. Taken together, these three properties make the TMM formulation particularly well suited to AFG tapered members with strongly varying material or geometric distributions, for which mesh-based approaches would require additional convergence studies.

Acknowledgments

The author thanks Trakya University, Department of Mechanical Engineering, for the academic environment in which this work was conducted.

Conflict of Interest

The author declares no conflict of interest.

Data Sharing Statement

The data that support the findings of this study are available from the author upon reasonable request.

Author Contributions

Vedat Taşkın: Conceptualization, methodology, software, validation, formal analysis, investigation, writing-original draft, writing- review and editing, visualization.

Hüseyin Can Kılınç: Methodology, validation, investigation, writing-review and editing.

Funding

This study did not receive any specific grant from funding agencies in the public, commercial, or not-for-profit sectors.

ORCID

Vedat Taşkın — 0000-0002-3013-2317

Hüseyin Can Kılınç — 0009-0009-5905-0647

References

Banerjee, J. R., & Ananthapuvirajah, A. (2019). Free flexural vibration of tapered beams. Computers & Structures, 224, 106106.

Birman, V., & Byrd, L. W. (2007). Modeling and analysis of functionally graded materials and structures. Applied Mechanics Reviews, 60(5), 195–216.

Boiangiu, M., Ceausu, V., & Untaroiu, C. D. (2014). A transfer matrix method for free vibration analysis of Euler-Bernoulli beams with variable cross section. Journal of Vibration and Control, 22(11), 2591–2602.

Calió, I., & Elishakoff, I. (2005). Closed-form solutions for axially graded beam-columns. Journal of Sound and Vibration, 280(3–5), 1083–1094.

Cao, D., Gao, Y., Yao, M., & Zhang, W. (2018). Free vibration of axially functionally graded beams using the asymptotic development method. Engineering Structures, 173, 442–448.

Elishakoff, I. (2004). Eigenvalues of Inhomogeneous Structures: Unusual Closed-Form Solutions. Boca Raton, FL: CRC Press.

Elishakoff, I., & Endres, J. (2005). Extension of Euler's problem to axially graded columns: Two hundred and sixty years later. Journal of Intelligent Material Systems and Structures, 16(1), 77–83.

Huang, Y., & Li, X. F. (2010). A new approach for free vibration of axially functionally graded beams with non-uniform cross-section. Journal of Sound and Vibration, 329(11), 2291–2303.

Kien, N. D., & Gan, B. S. (2014). Large deflections of tapered functionally graded beams subjected to end forces. Applied Mathematical Modelling, 38(11–12), 3054–3066.

Koizumi, M. (1997). FGM activities in Japan. Composites Part B: Engineering, 28(1–2), 1–4.

Lee, J. W., & Lee, J. Y. (2016). Free vibration analysis using the transfer-matrix method on a tapered beam. Computers & Structures, 164, 75–82.

Lee, J. W., & Lee, J. Y. (2020). Free vibration analysis of a rotating double-tapered beam using the transfer matrix method. Journal of Mechanical Science and Technology, 34(7), 2731–2744.

Ge, R., Liu, F., Wang, C., Ma, L., & Wang, J. (2022). Calculation of critical load of axially functionally graded and variable cross-section Timoshenko beams by using interpolating matrix method. Mathematics, 10(13), 2350.

Su, X., Hu, T., Zhang, W., Kang, H., Cong, Y., & Yuan, Q. (2024). Transfer matrix method for free and forced vibrations of multi-level functionally graded material stepped beams with different boundary conditions. Applied Mathematics and Mechanics, 45(6), 963–1000.

Pestel, E. C., & Leckie, F. A. (1963). Matrix Methods in Elastomechanics. New York: McGraw-Hill.

Rajasekaran, S., & Tochaei, E. N. (2014). Free vibration analysis of axially functionally graded tapered Timoshenko beams using differential transformation element method and differential quadrature element method of lowest-order. Meccanica, 49(4), 995–1009.

Reddy, J. N. (2017). Energy Principles and Variational Methods in Applied Mechanics (3rd ed.). Hoboken, NJ: John Wiley & Sons.

Sayyad, A. S., & Ghugal, Y. M. (2018). Modeling and analysis of functionally graded sandwich beams: A review. Mechanics of Advanced Materials and Structures, 26(21), 1776–1795.

Shahba, A., Attarnejad, R., & Hajilar, S. (2011). Free vibration and stability of axially functionally graded tapered Euler-Bernoulli beams. Shock and Vibration, 18(5), 683–696.

Shahba, A., Attarnejad, R., Tavanaie Marvi, M., & Hajilar, S. (2011b). Free vibration and stability analysis of axially functionally graded tapered Timoshenko beams with classical and non-classical boundary conditions. Composites Part B: Engineering, 42(4), 801–808.

Shahba, A., & Rajasekaran, S. (2012). Free vibration and stability of tapered Euler-Bernoulli beams made of axially functionally graded materials. Applied Mathematical Modelling, 36(7), 3094–3111.

Shampine, L. F., & Reichelt, M. W. (1997). The MATLAB ODE Suite. SIAM Journal on Scientific Computing, 18(1), 1–22.

Singh, K. V., & Li, G. (2009). Buckling of functionally graded and elastically restrained non-uniform columns. Composites Part B: Engineering, 40(5), 393–403.

Soltani, M., & Asgarian, B. (2019). New hybrid approach for free vibration and stability analyses of axially functionally graded Euler-Bernoulli beams with variable cross-section resting on uniform Winkler-Pasternak foundation. Latin American Journal of Solids and Structures, 16(3), e173.

Storch, J., & Elishakoff, I. (2018). Buckling of axially graded columns: A fifth-order polynomial mode shape. AIAA Journal, 56(6), 2509–2513.

Timoshenko, S. P., & Gere, J. M. (1961). Theory of Elastic Stability (2nd ed.). New York: McGraw-Hill.

Zarrinzadeh, H., Attarnejad, R., & Shahba, A. (2011). Free vibration of rotating axially functionally graded tapered beams. Proceedings of the Institution of Mechanical Engineers, Part G: Journal of Aerospace Engineering, 226(4), 363–379.